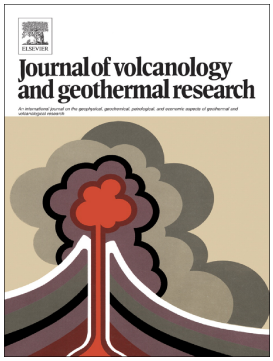

Exploring deformation scenarios in Timanfaya volcanic area (Lanzarote, Canary Islands) from GNSS and ground based geodetic observations

U. Riccardi, J. Arnoso, M. Benavent, E. Vélez, U. Tammaro, F.G. Montesinos

PII: S0377-0273(18)30036-2
DOI: doi:10.1016/j.jvolgeores.2018.04.009
Reference: VOLGEO 6352

To appear in: *Journal of Volcanology and Geothermal Research*

Received date: 26 January 2018
Revised date: 7 April 2018
Accepted date: 9 April 2018

Please cite this article as: U. Riccardi, J. Arnoso, M. Benavent, E. Vélez, U. Tammaro, F.G. Montesinos , Exploring deformation scenarios in Timanfaya volcanic area (Lanzarote, Canary Islands) from GNSS and ground based geodetic observations. The address for the corresponding author was captured as affiliation for all authors. Please check if appropriate. Volgeo(2017), doi:10.1016/j.jvolgeores.2018.04.009

EXPLORING DEFORMATION SCENARIOS IN TIMANFAYA VOLCANIC AREA (LANZAROTE, CANARY ISLANDS) FROM GNSS AND GROUND BASED GEODETIC OBSERVATIONS

U. Riccardi [a,d)*], J. Arnoso [b,d)], M. Benavent [c,d)], E. Vélez [b,d)], U. Tammaro [e)] and FG. Montesinos [c,d)]

[a)] Dipartimento di Scienze della Terra, dell'Ambiente e delle Risorse (DiSTAR), University "Federico II" of Naples, Italy

[b)] Instituto de Geociencias (IGEO, CSIC-UCM). C/ Doctor Severo Ochoa, 7. Facultad de Medicina (Edificio Entrepabellones 7 y 8). 28040 Madrid, Spain

[c)] Facultad de Matemáticas, Universidad Complutense de Madrid, Plaza de Ciencias 3, 28040 Madrid, Spain

[d)] Research Group 'Geodesia', Universidad Complutense de Madrid, Spain

[e)] Istituto Nazionale di Geofisica e Vulcanologia, Italy

[*] **corresponding author**: umbricca@unina.it, Phone: +39 0812538350; Largo S. Marcellino, 10, 80138 Napoli (Italy)

ABSTRACT

We report on a detailed geodetic continuous monitoring in Timanfaya Volcanic Area (TVA), where the most intense geothermal anomalies of Lanzarote Island are located. We analyze about three years of GNSS data collected on a small network of five permanent stations, one of which at TVA, deployed on the island, and nearly 20 years of tiltmeter and strainmeter records acquired at Los Camelleros site settled in the facilities of the Geodynamics Laboratory of Lanzarote within TVA.

This study is intended to contribute to understanding the active tectonics on Lanzarote Island and its origin, mainly in TVA. After characterizing and filtering out the seasonal periodicities related to "non-tectonic" sources from the geodetic records, a tentative ground deformation field is reconstructed through the analysis of both tilt, strain records and the time evolution of the baselines ranging the GNSS stations. The joint interpretation of the collected geodetic data show that the area of the strongest geothermal anomaly in TVA is currently undergoing a SE trending relative displacement at a rate of about 3 mm/year. This area even experiences a significant subsidence with a maximum rate of about 6 mm/year. Moreover, we examine the possible relation between the observed deformations and atmospheric effects by modelling the response functions of temperature and rain recorded in the laboratory. Finally, from the retrieval of the deformation patterns and the joint analysis of geodetic and environmental observations, we propose a qualitative model of the interplaying role between the hydrological systems and the geothermal anomalies. Namely, we explain the detected time correlation between rainfall and ground deformation because of the enhancement of the thermal transfer from the underground heat source driven by the infiltration of meteoric water.

Keywords: Timanfaya volcanic area, Geodetic monitoring, GNSS, Tiltmeter, Strainmeter, Ground deformation scenario

1. INTRODUCTION

1.1 Problem setting and aims

Geodetic data from both terrestrial and space techniques are commonly acquired in active volcanic areas to identify precursory signals and infer the knowledge of plumbing system through the modelling of ground deformations (e.g. Battaglia et al., 2003a; 2003b; Puglisi et al., 2001; Dzurisin, 2003, 2007; Sturkell et al., 2006; Crescentini and Amoruso, 2007; Chang et al., 2010; Grapenthin et al., 2013; Sainz-Maza et al., 2014; Le Mével et al., 2015; Fernández et al., 2015). In principle, frequent geodetic surveys of networks allow to characterize the deformation field in space and time, but not continuously, preventing from keep pace with a rapidly evolving volcanic unrest. Hence, continuous geodetic monitoring has a key role in both active and quiescence periods, because it can provide a dense time series of data even for a real time analysis (Dzurisin, 2007). GNSS, tiltmeters and strainmeters are widely used to continuously monitor ground deformations related to volcanic activity and to investigate the stages of eruptive processes (e.g., Owen et al., 2000; Widiwijayanti et al., 2005; Dzurisin, 2007; Bonaccorso et al., 2002, 2009, 2013; Arnoso et al., 2012a; Montgomery-Brown et al., 2011; Newman et al., 2012; Tammaro et al., 2013; Amoruso et al., 2015; Gambino et al., 2016). Even during quiescence periods or preparatory stages of eruption, continuous geodetic observations can help to assess volumes of magma accumulation beneath active volcanoes, as they can resolve small tilts and ground deformations. For instance, Amoruso et al. (2015) through the analyses of high sensitivity strain and tilt measurements shed light on the sources of the ground inflation/deflation and seismicity in Campi Flegrei caldera (Italy).

Here we use continuous GNSS observations collected on 5 stations deployed over Lanzarote island as well as geodetic measurements carried out at the Geodynamics Laboratory of Lanzarote (GLL) (Fig. 1).

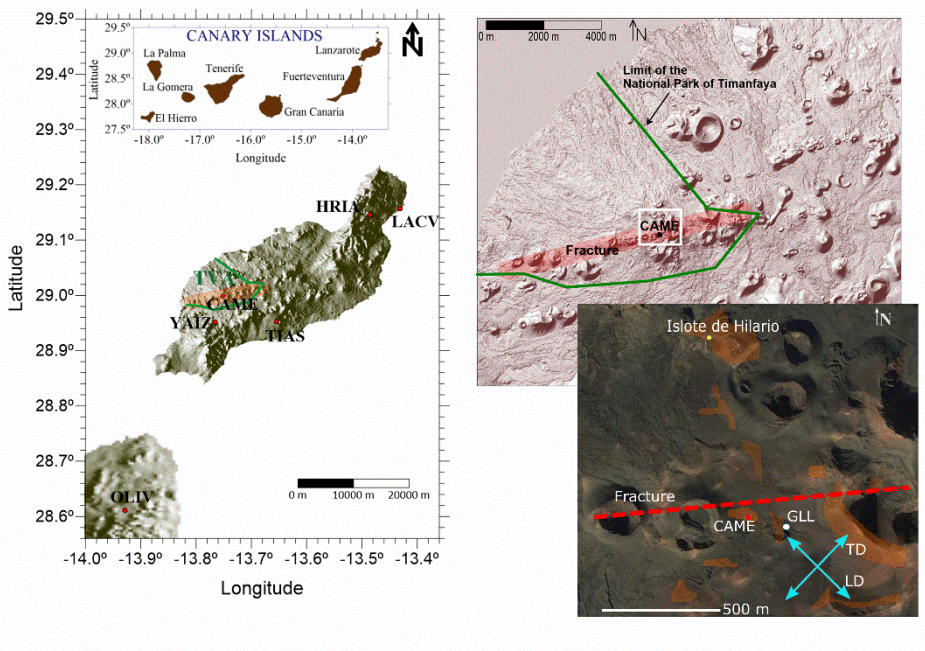

Fig. 1: (Left) Shaded relief map of Lanzarote Island, located in the Canary Islands (inlet), showing the limits (green line) of Timanfaya National Park, the fissure zone (shaded orange area) of the 1730-1736 volcanic eruption and the location of GNSS stations. (Up-Right) Zoomed relief map of the Timanfaya volcanic area (TVA) indicating the position of the GNSS station CAME. (Down-Right) The squared area is a Google Earth image that shows the main thermal anomalies (in orange color) located in the area close to Islote de Hilario (according to Araña et al., 1984), the position of the 13 m deep well (yellow circle) having more than 600 ºC and the Geodynamics Laboratory of Lanzarote (GLL) at the TVA. The two orthogonal lines (LD, TD) represent the respective orientation of the strainmeters and tiltmeters at GLL site.

The GLL has ground-based instruments to observe tilts, deformations and displacements in continuous operating mode, which are located at different observing sites along the island. In particular, two main installations are respectively inside the lava tunnel of La Corona volcano (NE sector), and right above the largest heat flow anomaly of the island (SW sector) at the Timanfaya volcanic area (TVA); we will refer to the latter as “Laboratory of Camelleros” (LC-GLL). In short, as shown by a number of authors (e.g. Vieira et al., 1991; Fernández et al., 1992; Arnoso et al., 2001a, 2001b, 2011), the laboratory meets the experimental conditions to observe and study geodetic and geophysical parameters in a volcanic active area and, in particular, it allows the interpretation of geophysical signals of volcanic origin during periods of quiescence.

The main goal of this study is the interpretation of the ground deformations detected at TVA, where the most intense thermal anomalies take place. To benefit from a wide range of geodetic detectability, here we analyze GNSS data, recorded from 2014 to 2017 on a small network spanning the island as well as long records from strainmeters and tiltmeters operating at LC-GLL. Moreover, through the deformation

patterns and the analysis of the environmental observations (air temperature and rain) we target to shed light on the possible interplaying role between the hydrological system and the thermal anomalies. Based on the modeling of the transfer functions of environmental and geodetic data we attain a qualitative model involving meteoric water infiltration towards the buried heat source as the trigger of the observed ground deformations.

1.2 Geodynamical and Volcanological framework

Canary Islands are an intraplate oceanic volcanic archipelago consisting of seven major islands and four islets about 500 km extended from East to West (Fig. 1). Radiometric dating and magnetic stratigraphy confirm an east-to-west age progression of subaerial volcanism, stretching from 25 Ma for Fuerteventura and Lanzarote islands to 1 Ma for El Hierro (Carracedo and Troll, 2016; Dañobeitia and Canales, 2000; Guillou et al., 1996; McDougall and Schmincke, 1976; Abdel Monem et al., 1972). The archipelago is volcanically active and all the islands (except La Gomera) exhibit Holocene volcanism. The last eruption in Canary Islands was a submarine event off shore El Hierro that began on October 10, 2011 and ended at the beginning of March 2012 (López et al., 2012). Due to some peculiarities in geochemistry and geochronology of the rocks as well as the geodynamic complexity and tectonics, the origin of the archipelago from a hot spot is still debated. Indeed, the archipelago is the result of long-term volcanic and tectonic activity, which started around 60 Ma. Several hypothesis concerning its origin have been formulated to date, as the hot spot (Morgan, 1971; Wilson, 1963), the propagating fracture (Anguita and Hernán, 1975), the local extensional ridge (Fúster, 1975) and the set of uplifted tectonic blocks (Araña and Ortiz, 1991). The most accepted model is the unifying one by Anguita and Hernán (2000), which explains the time-space magmatism and the uplift of the archipelago as due to a remnant mantle thermal anomaly underneath Canary Islands, North Africa and Western Europe tapped by the fractures inherited from the Mesozoic aborted arm rift. The main directions of fractures in the islands are related to both the opening of the mid-Atlantic ridge and the tectonics of the Atlas range (Mezcua et al. 1992). Namely, the WNW-ESE direction corresponds to the so called "*Atlantic trend*", while the NNE-SSW and ENE-WSW directions correspond to the "*African trend*". Moreover, the ENE-WSW trend agrees with the alignment of eruptive vents during the historical eruptions in Lanzarote

Island. Recently, López et al. (2017) have pointed out an increase in tectonic activity in the Canary Islands region since year 2003, induced by the ponding of Canarian mantle plume. As a result, drifting East-West extensional and uplift deformations were observed in the region. Accordingly, vertical velocities of about 1 mm/year and 0.7 mm/year and horizontal velocities of about 2 mm/year and 0.5 mm/year are retrieved in the European and African frames respectively.

The island of Lanzarote is located to the northeast of the Canarian Archipelago. The most relevant eruption of the last 500 years took place during 1730 to 1736, giving rise to more than 30 volcanic cones. The eruptive vents are aligned along a system of parallel fractures of about 14 km in length trending N70°E (Fig. 1) along the path of the central structural rift-type zone (Carracedo et al., 1992). Other eruptions occurring in year 1824, with 3 new volcanoes emerged and aligned in the same direction. Fissural eruptions and low-explosive basaltic magmas characterized all this eruptive activity. The TVA is a volcanic field located at the southwest of Lanzarote, covering most of the land extension generated during the 1730-1736 eruption. Presently, thermal anomalies are located at TVA, and they are confined either in fracture-related alignments or along craters' rim. The temperature recorded ranges to a maximum of 605 ºC, as measured inside a slightly inclined 13 m deep well located at Islote de Hilario site (see Fig. 1). Remnant hot magma at approximately 4 km depth that fed the 1730–1736 eruption explains the thermal anomalies (Carracedo and Troll, 2016), hence, their deep origin is from an intrusive magma body undergoing a cooling process, but still having a very high temperature. Araña et al. (1984) suggested that thermal energy is transported through the fractures by magmatic volatiles and/or by water vapour coming from a deep-seated 3–4 km water table. Indeed, the lack of enough proportion of volcanic gases requires the assumption of water tables in contact with or near to intruded magma bodies to explain how heat causes the water to rise. Díez-Gil et al. (1987) modelled this type of thermal anomaly from a convective system. They argued that if the cooling time for basaltic magmas in the chambers is about 10^4 - 10^5 years, variations in the water tables could explain the possible variations in surface anomalies.

2. DATA SET AND STRATEGY OF DATA ANALYSIS

2.1 Continuous GNSS data

In late April 2014, a new permanent GNSS station has been installed in TVA for an improved geodetic monitoring of the zone of highest geothermal anomalies of the island, near the LC-GLL (Fig. 1). This station hereafter referred as CAME has been jointly supported by the Institute of Geosciences (CSIC-UCM), Dipartimento di Scienze della Terra dell'Ambiente e delle Risorse (DiSTAR) of the University "Federico II" of Napoli and the Geodesy Research Group of University Complutense of Madrid (GRG-UCM). Besides the records from CAME we collect data from 4 permanent stations spread over Lanzarote island (HRIA, LACV; TIAS, YAIZ) plus OLIV located on Fuerteventura island (Fig. 1), which is reportedly tightly related to Lanzarote from geologic point of view (Hoenrle and Carracedo, 2009). Different institutions manage the GNSS stations, as follows: CAME is co-operated by CSIC-UCM and DiSTAR; LACV is managed by (CSIC-UCM and GRG-UCM); stations HRIA, TIAS, YAIZ and OLIV belong to GRAFCAN (Cartographical Service of the Government of Canary Islands).

The GNSS data set analyzed in this paper consists of about 1000 days collected since installation of CAME and spanning 9 May 2014 - 31 January 2017 time interval. We process the small Lanzarote network in a larger one formed by twelve IGS stations, 10 of them are even ITRF08 (Altamimi et al. 2011) reference stations (Tab. 1).

Lanzarote GNSS Network

Name	**Location**	**Lat. (°)**	**Long. (°)**	**Ellipsoidal Height (m)**
CAME	Camelleros (TVA)	28.99862	346.24878	398.920
LACV	Casa de los Volcanes	29.15715	346.56876	71.197
HRIA	Haria	29.14523	346.51489	319.874
TIAS	Tías	28.95214	346.34573	258.793
YAIZ	Yaiza (TVA)	28.95184	346.23449	233.531
OLIV	La Oliva (Fuerteventura)	28.61042	346.07132	270.506

Regional GNSS Network

LPAL	La Palma (Tenerife, Spain)	28.76387	342.10617	2199.178
MAS1	Maspalomas (Gran Canaria, Spain)	27.76374	344.36673	197.116
MATE	Matera (Italy)	40.64913	16.70446	535.662
NOT1	Noto (Italy)	36.87585	14.98979	126.339
GRAS	Caussols (France)	43.75474	6.92058	1319.316
GRAZ	Graz-Lustbuehel (Austria)	47.06713	15.49348	538.291
SFER	San Fernando (Portugal)	36.46435	353.79436	84.153
PDEL	Ponta Delgada (Azores, Portugal)	37.74775	334.33724	110.601
RABT	Rabat (Marocco)	33.99811	353.14571	90.084
WTZR	Wettzell (Germany)	49.14420	12.87891	666.027

YEBE	Yebes (Spain)	40.52490	356.91138	972.758
ZIMM	Zimmerwald (Switzerland)	46.87710	7.465308	956.347

Tab. 1. Location sites of the permanent GNSS stations used for this study.

GNSS data are analyzed with Gamit-Globk v.10.6 (Herring et al., 2015a; 2015b) software using IGS final precise orbits to process data. IGS absolute phase center variation for the satellite/receiver antennas is applied and 10° is set as elevation cut off for the network observations. Angle elevation dependent weighting have been applied as well. The GPT2 global tropospheric delay model (Lagler et al., 2013) is used to generate a priori values for the tropospheric delay, but total troposphere slant delay has been estimated for all the stations every two hours through the Vienna mapping functions "VMF1" (Boehm et al. 2006). The ionosphere effect is reduced by using the "LC" ionosphere-free linear combination phase as observables. The ocean tide loading effect is accounted according to FES2004 model (Lyard et al., 2006). Primary GNSS observations in RINEX format, collected along 24 hours continuous sessions, with 30 seconds sampling rate, are processed with Gamit. These primary solutions ("quasi-observations") are performed with loose a priori uncertainties assigned to the global parameters, so that constraints can be applied uniformly in both daily and combined solutions (Dong et al. 1998). Quasi-observations, namely estimates for station coordinates, earth-rotation parameters, orbital parameters, and source positions and associated covariance matrices, are used as primary data input of the Kalman filter implemented in Globk. The Lanzarote network is adjusted in the ITRF08 reference frame through the "generalized" approach as described by Dong et al. (1998), by using 10 IGS/ITRF08 stations (MATE; NOT1; GRAS; GRAZ; SFER; PDEL; RABT; WTZR; YEBE; ZIMM) (Table 1). Due to the small size of the network, as Helmert transformation, we assess just translation, without rotation and scale parameters; results of datum realization are listed in Table 2. Daily solutions (coordinates) and normal equations are calculated and subsequently combined by Globk in order to obtain 15 days solutions for all the stations. Linear regression trends derived from coordinate time series are just accounted for as a first approximation for absolute velocities in ITRF08, but more accurate results are achieved after annual and semi-annual seasonal effects were calculated as well as outliers were removed. We identified and accounted for discontinuities in the time series due to antenna changes in most of the cases.

Position System Stabilization		
	Translation (m)	Standard deviation (m)
X	+ 0.132	± 0.016
Y	- 0.129	± 0.008
Z	- 0.155	± 0.015

Tab. 2. Helmert transformation (just translation) assessed for Lanzarote network; results after 4 iterations.

The three topocentric components (k = North, East, Up) time series, sampled at discrete times t_i, are modelled by a least-squares fitting independently applied to each site through the following conceptual equation (Nikolaidis, 2002), which represents the position components $Y_k(t_i)$:

$$Y_k(t_i) = a + v_k(t_i - t_0) + \sum_{p=1}^{2} a_p \sin(2p\pi t_i) + \sum_{p=1}^{2} b_p \cos(2p\pi t_i) + \sum_{l=1}^{L} d_l \Theta(t_l - t_0) + \varepsilon_i \quad (1)$$

where, a is the station position at time t_0, v_k is the velocity of the k component, the linear rate (slope); a_1, b_1, a_2, b_2 are the annual and semi-annual amplitudes respectively, d_l are jumps (offsets, steps, discontinuities), which are due to real deformation and/or more likely instrumental changes at epoch t_l, Θ is the Heaviside function, ε_i is the noise term. For a realistic accounting of noise and related errors in the computed velocities, we use the "realistic sigma" algorithm (Herring, 2003). Studies on long-term GNSS coordinate time series have shown that formal velocity error statistics, estimated with a standard least square algorithm, underestimate the actual values, hence temporal correlations in the data might be accounted for (Williams et al., 1998). This spectral feature has been attributed to the instability of geodetic monuments. Indeed such correlations in the time series could mask or bias the underlying geophysical signal. In particular, power spectral analysis of post-fit residuals shows that noise over periods of a few days is nearly white, but increases for longer periods, resembling a random walk process, often referred to as 'red' or 'brown' noise (Williams et al., 2004). In the daily solutions, just a least square linear trend is assessed (Fig. 2), while in the 15-days combined time series both linear and seasonal periodicities are reduced (Fig. 3). The filtering out of the linear and periodical trends is done through a least square fitting after a retrieval of sine and cosine terms with specified periods (annual: 365.24 days and semestral: 182.62 days); as expected, we retrieve significant seasonal effects just on vertical components. After filtering out the outliers from the time series, namely by

rejecting solutions having repeatability larger than 2σ, we retrieve both the baselines among the stations and the horizontal velocity vectors (Fig. 5 and Tab. 3). The time evolution of the baselines ranging from CAME to all of the stations in Lanzarote network is studied (Fig. 4); the detected trends are discussed in the following section (see Sect. "3 Discussion"). The horizontal velocities are reproduced in both ITRF08 and "local" frames for each stations of the network. Local frame for our small network, located on Africa plate, is realized by subtracting the velocity assessed at TIAS station (23.7 mm/year N 43° E) being coherent with the Africa plate according to NUVEL-1A model (De Metz et al., 1994). The assessment of a local velocity field is aimed at eliminating the global tectonic motion of the plate to emphasize, if any, the local tectonics.

As discussed later, the most relevant outcomes from the GNSS velocities is a residual vector at CAME trending about 150° SE (Fig. 5b), which implies a shortening trend in CAME-TIAS baseline time evolution (Fig. 4c).

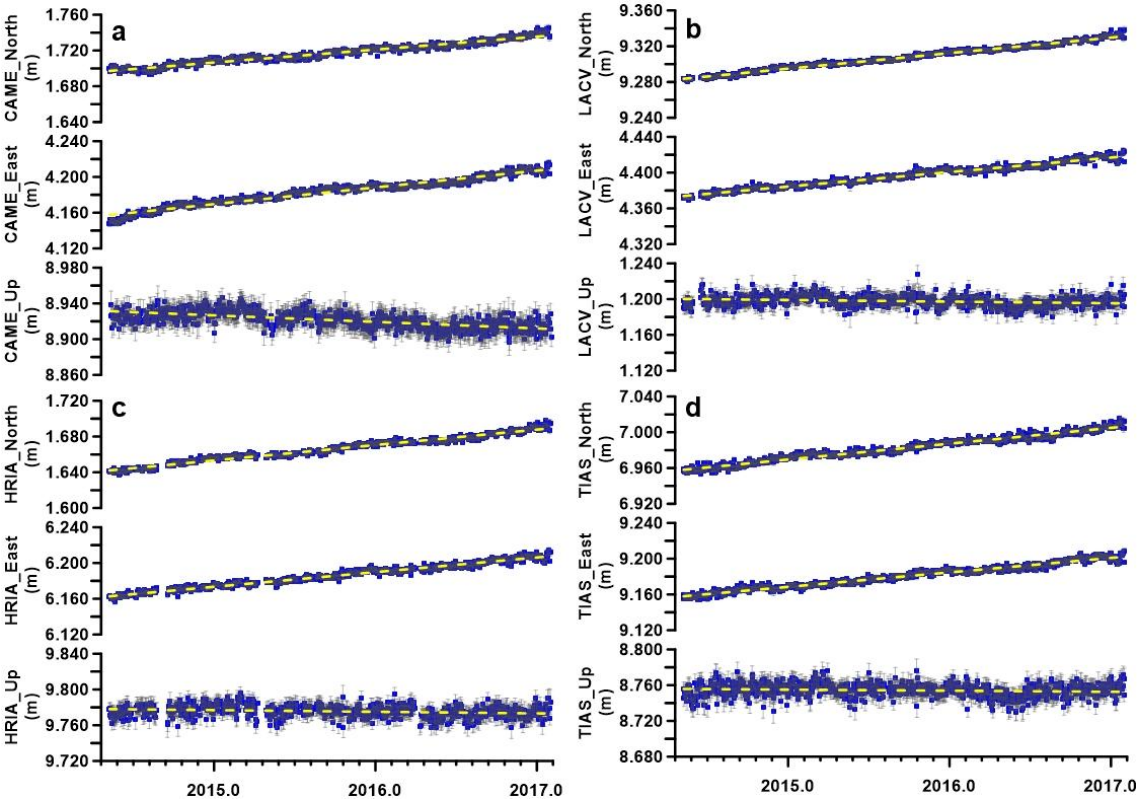

Fig. 2: Daily time series of the GNSS permanent stations in the framework of the ITRF08 reference system; the yellow dashed lines represent the linear fitting.

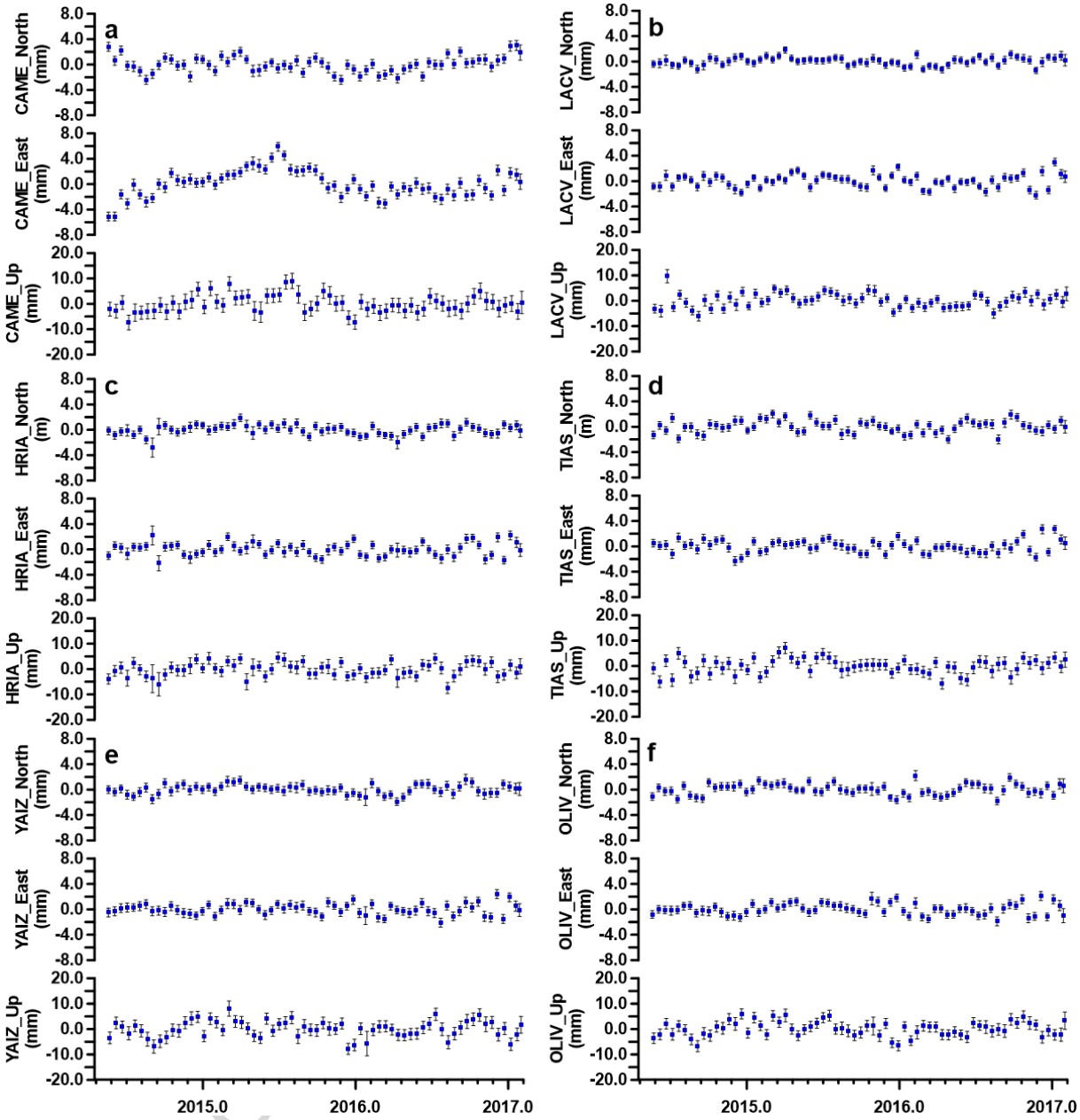

Fig. 3: 15-days combined time series of residual positions after removal of linear, annual and semestral trends.

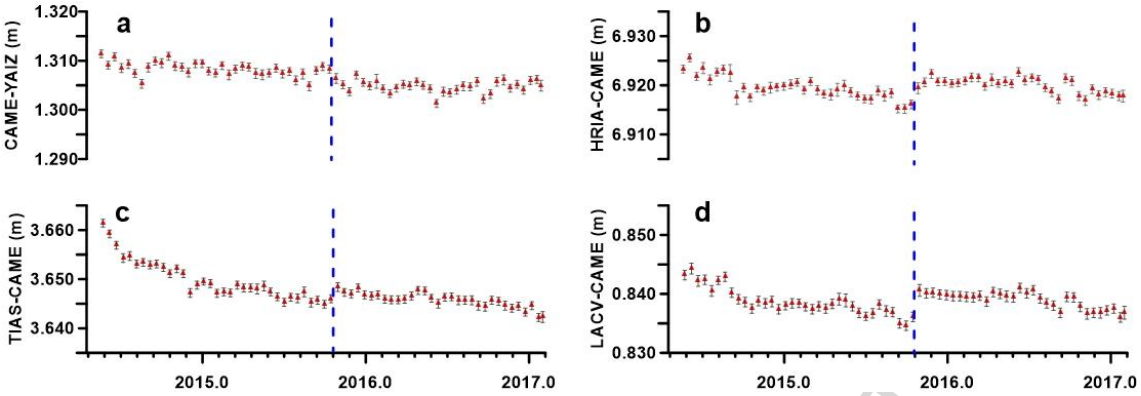

Fig. 4: 15 days combined time series of the baselines inter-ranging between CAME and the other stations on Lanzarote island after filtering out the annual and semestral trends. The blue dashed lines mark the time of the monumentation change at CAME.

Site Id.	T. Serie Length (year)	ITRF08_N (mm/year)	ITRF08_E (mm/year)	ITRF08_Up (mm/year)	wrt TIAS_N (mm/year)	wrt TIAS_E (mm/year)
CAME	2.79	14.21 ± 1.11	18.53 ± 1.24	-6.14 ± 1.65	-3.26	2.60
LACV	2.79	17.23 ± 0.67	16.11 ± 1.07	-0.53 ± 1.81	-0.15	-0.06
HRIA	2.79	16.91 ± 0.77	16.24 ± 1.02	-0.94 ± 1.23	-0.35	-0.05
TIAS	2.79	17.39 ± 1.00	16.08 ± 1.04	-0.30 ± 1.63	***	***
YAIZ	2.79	17.15 ± 0.75	16.36 ± 0.89	-2.06 ± 1.61	-0.41	0.38
OLIV	2.79	16.50 ± 0.89	16.73 ± 0.92	-0.32 ± 1.82	-1.12	0.95

Tab. 3. Horizontal and Up velocities represented in ITRF08 and relative horizontal velocities computed with respect to TIAS; coordinates of the sites are given in Tab. 1.

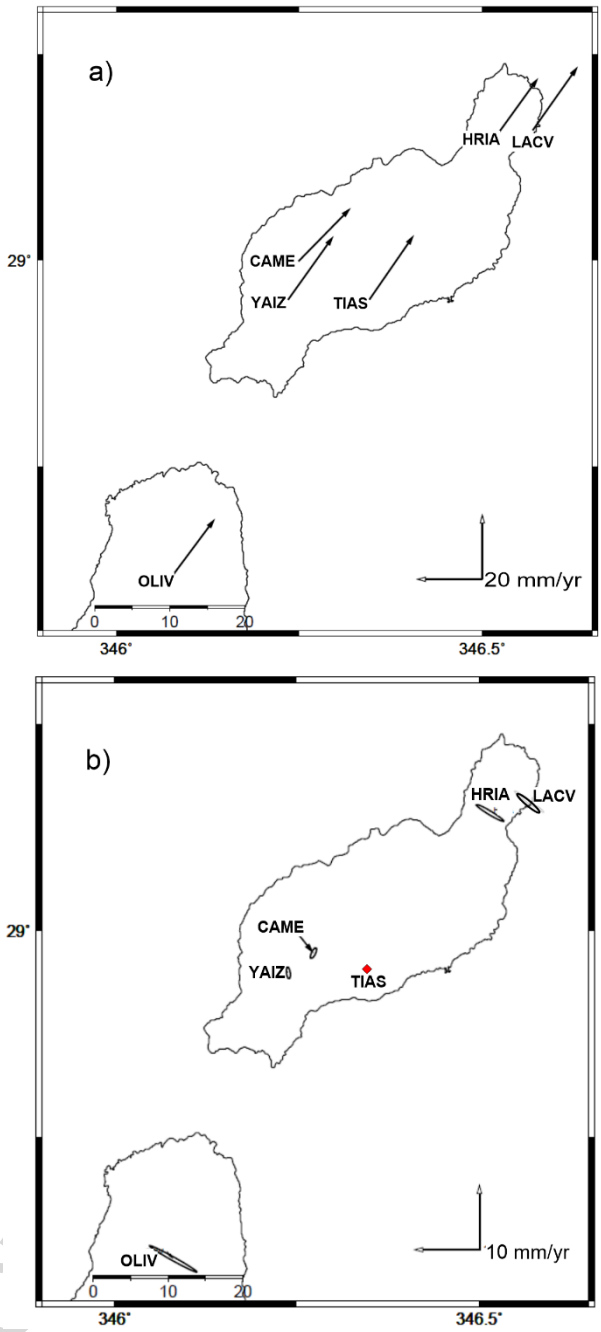

Fig. 5: Velocity solutions retrieved from CGNSS data collected on Lanzarote Island from May 2014 to December 2016 with respect to two different frames: ITRF08 (a) and local (b).

2.2 Continuous strainmeter and tiltmeter data

Tiltmeters and strainmeters used in this study are installed in the LC-GLL, at the TVA enclosure. The laboratory consists of an underground construction placed 3 m below the ground level, having two orthogonal tunnels, 0.8 m deep and about 12 and 6 m long, running in longitudinal (LD) and transversal (TD) directions respectively (Fig.

1). The tunnels host the observing instruments for tilt and strain measurements (Vélez et al., 2001; Arnoso et al., 2001b; Vieira and Vélez, 2006).

We use 1-minute data samples from two orthogonal strainmeters (EXT557 and EXT775) built through several assembled ceramic tubes, and having a special copper thread fastened to an aluminum frame attached to various pillars distributed along the tunnels. One of the strainmeter ends is attached to the ground and supports a micrometer screw for calibrations, the other one measures the displacements through a magnetic sensor equipped on the tube. It is well know that variations in the local rheology and elastic coupling between the instrument and the rock can cause variations in the sensitivity of the instrument (Zadro and Braitenberg, 1999). Thus, in situ calibrations are performed biannually to retrieve the calibration factor in terms of displacement units (μm), and then the relative deformation expressed as dimensionless strain dl/L (1 nstr = 10^{-9}), L being the baseline length of the strainmeter. A positive dl means elongation, namely an increase in the length L. The relative variations of length (dl/L) are found with a sensitivity of 1 nstr and the calibration factors are computed within a range of 0.3×10^{-9}

The two tiltmeters (PV602 and PV603) are uniaxial vertical pendulums orthogonally set up, each one mounted on a short base platform equipped with levelling screws. The mass hangs from a thin plate, and oscillates inside a stainless steel box refilled with oil to dump the high frequency noise. A capacitive sensor detects the displacement between the mass and the plate fixed to the frame of the instrument. As for the strainmeters, calibrations are performed biannually. The tilts are found with a sensitivity of 0.1 and 0.2 μrad for the PV602 and PV603 pendulums respectively, and the calibration factors are computed within a range of 0.02 μrad for both instruments (Arnoso et al., 2001b).

The time evolution of the strain and tilt signal in LD and TD directions, and their respective rates of annual variation is quite characteristic (Fig. 6). We can clearly observe that tilt and strain data are dominated by long term fluctuations at different time scales, typically from months to years.

Moreover, by jointly plotting the residual tilts, after removing tides and room temperature effects at tidal frequencies, from the two orthogonal vertical pendulums, we obtain the tilt trace (Fig. 7) for the same period of GNSS observations at CAME. The trace (red line in Fig. 7) indicates that the predominant tilt during such time span is about 153º N, which more or less coincides with the direction of the relative velocity

vector computed for CAME, the GNSS station closest to LC-GLL, when it is calculated by fixing TIAS site (Figs. 5b and 7). To better investigate the linearity of the tilt evolution over the common time period spanning the GNSS data, we compute the fitting for different data clusters (color-coded in Fig. 7) according to date. When computing the linear trends for the different periods of observation regarding the annual variation (May 2014 to January 2017), we can observe that the respective azimuths are varying from 125º to 150º. That means that the tilt motion is not linear and, thus, the direction of the trend can change for a few amount, although it is always close to the total trend (153º) and to the velocity vector (150º) given by the GNSS at CAME site.

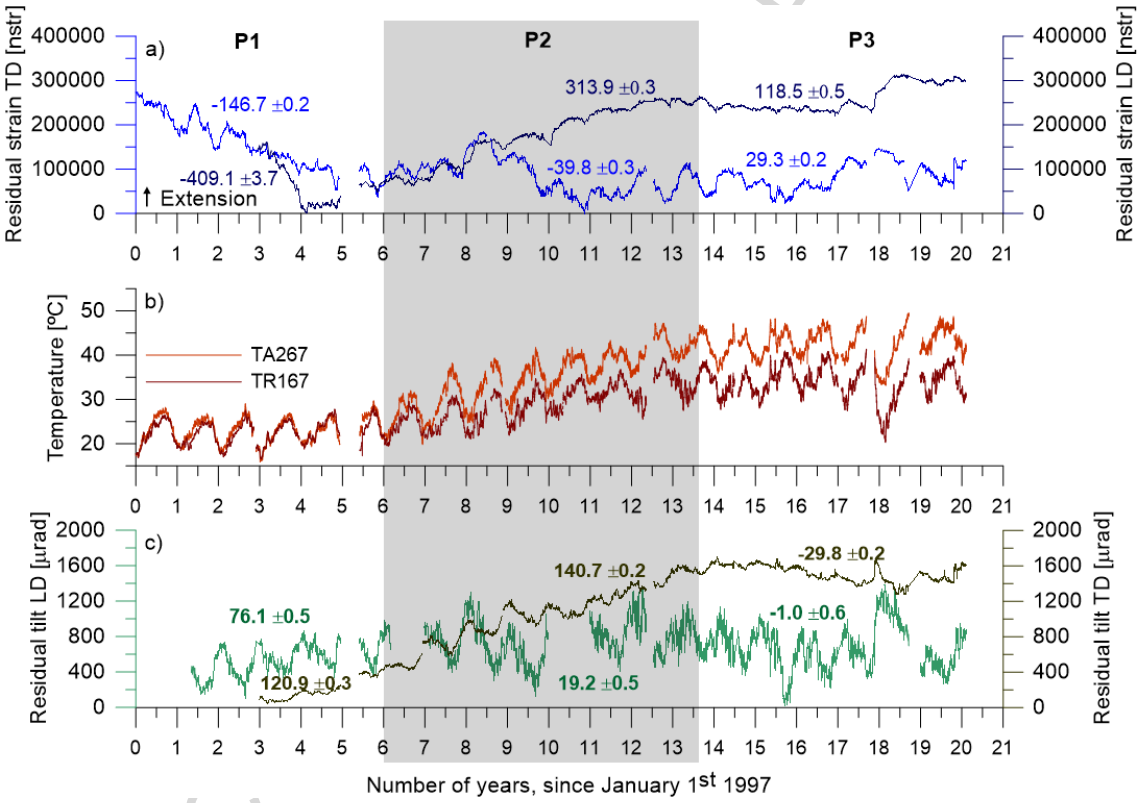

Fig. 6: Strain and tilt data (after removing diurnal tides) recorded in the two orthogonal directions (LD and TD at LC-GLL), located in the TVA (a, c). Air temperature (b) recorded in two different sites inside the LC-GLL. Shadow area shows the interval of 7 years of air temperature increasing in the laboratory. Strain/tilt rate values are even indicated as insets in deformation units [µm/year] and [µrad/year], respectively.

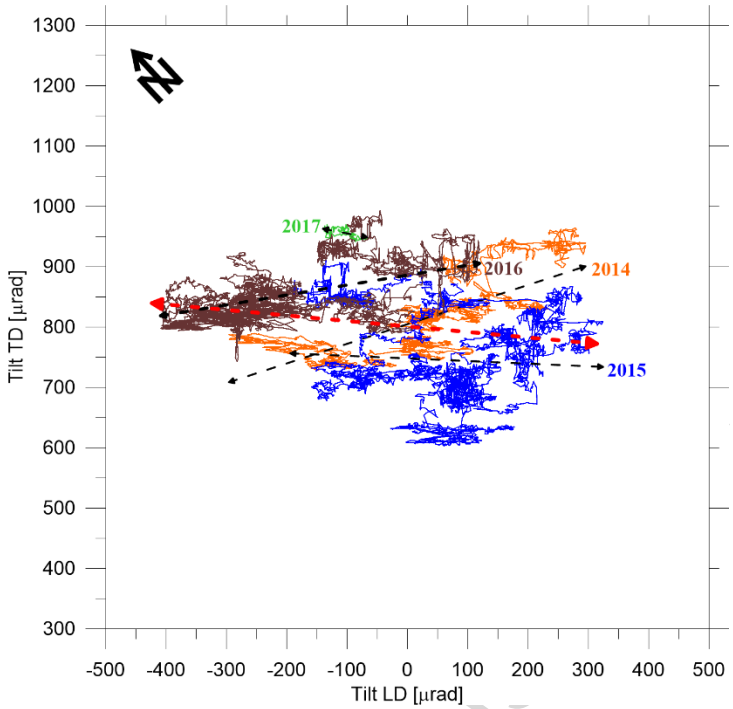

Fig. 7: Trace plot of the residual tilt signal (directions TD and LD) after subtracting tidal and air temperature effects at tidal frequencies. The colors represent the trace for the year 2014 (orange), 2015 (blue), 2016 (brown) and 2017 (green). The black dotted lines are the linear fit of the trace for the respective year. The red dashed red line is a linear fit of the trace for the overall period of observation. The standard deviation of the fit is 73.5 µrad and the R^2 coefficient is of 0.04. Although the fit it is not very significant, the adjusted line is shown to point more clearly the predominant direction of tilt during the observing period.

In a bid to understand the main features of the time evolution of both tilt and strain signals, we do a correlation analysis between the geodetic records and the environmental parameters (room temperature and rain) collected in LC-GLL. The idea behind this approach is that the observed seasonal variations represent ground deformations having thermoelastic origin toughly controlled by temperature and rain. Therefore, as done for GNSS data, it is reasonable to decompose these fluctuations into periodic seasonal variations as well as a polynomial trend. In this regard, ground deformation data are modelled using a regression approach after removing the effects of tides, by considering a linear relation with temperature as follows (Venedikov et al., 2006):

$$S(t) = E_T(t) + P(t),\ t = t_1, t_2, \dots t_n \qquad (2)$$

S(t) being the tilt, strain or displacement signal having a deformation component induced by the temperature $E_T(t)$, which is expressed in terms of a unknown regression coefficient, *R*, and a time lag, Δ*t*. That is,

$$E_T(t) = R(T(t - \Delta t) - T_m) \quad (3)$$

where, T_m is the mean value of the air temperature *T*(*t*). *P(t)* in equation (2) is a polynomial function which represents the residual drift model including geophysical and instrumental effects. Here we assume that polynomials are continuous functions with continuous derivatives over the data series, and expressed as

$$P(t) = \sum_{k=0}^{K} c_k t_k \quad (4)$$

with unknown c_k coefficients, *K* is the maximum polynomial order. A least squares approach allows estimation of the parameters c_k and *R*.

The values obtained for the regression coefficient *R* for the tilt and strain measurements are listed in Table 4; they show the modeled effect of the air temperature variations on the tilts and strains during all the period of observations available at LC-GLL.

Period	**EXT557 TD** (µm/ºC)*	**EXT775 LD** (µm/ºC)*	**PV603 TD** (µrad/ºC)	**PV602 LD** (µrad/ºC)
P_1	**-4.4±0.2**	**-6.6±0.7**	**-4.1±0.1**	**-36.1±0.3**
P_2	**-15.2±0.2**	**12.9±0.3**	**-21.3±0.1**	**3.4±0.1**
P_3	**-9.8±0.7**	**-22.5±1.0**	**-3.6±0.3**	**-38.4±1.5**

**Values are given in deformation units*

Tab. 4: Regression coefficients (R) calculated according to equation (3), showing the effect of the air temperature variations on both tilt and strain measurements for the different periods (P1, P2, P3) indicated in Figure 6.

An alternative source of ground deformation even co-working with temperature could be rain. A rain-induced ground deformation model is usually adopted (Kümpel et al., 2001) as a combination of either surface loading, thermoelastic strains produced by

changes in ground temperature, swelling of the soil due to moisture variation or by poroelastic strains produced by pore pressure effect. Because the amount of rain is low and happens in localized epochs (autumn season typically), we modelled a cumulative rainfall function through the following equation (Langbein, 1990; Crossley et al., 1998):

$$f_i = \sum_{k=1}^{i} r_k \left(1 - e^{-\frac{t_i - t_k}{\tau_1}}\right) e^{-\frac{t_i - t_k}{\tau_2}} \qquad (5)$$

In this expression, r_k is the amount of rain at time t_k. The time constants τ_1 and τ_2 describe the infiltration of the water into the ground and the dry out by evapotranspiration and downward migration, respectively.

Rain data were collected at a meteorological station located about 100 m far from CAME GNSS site. The rain function, modeled using equation (5), evidences that episodic rainfalls induce vertical displacements (Up component) during the rainy seasons (highlighted in Fig. 8a).

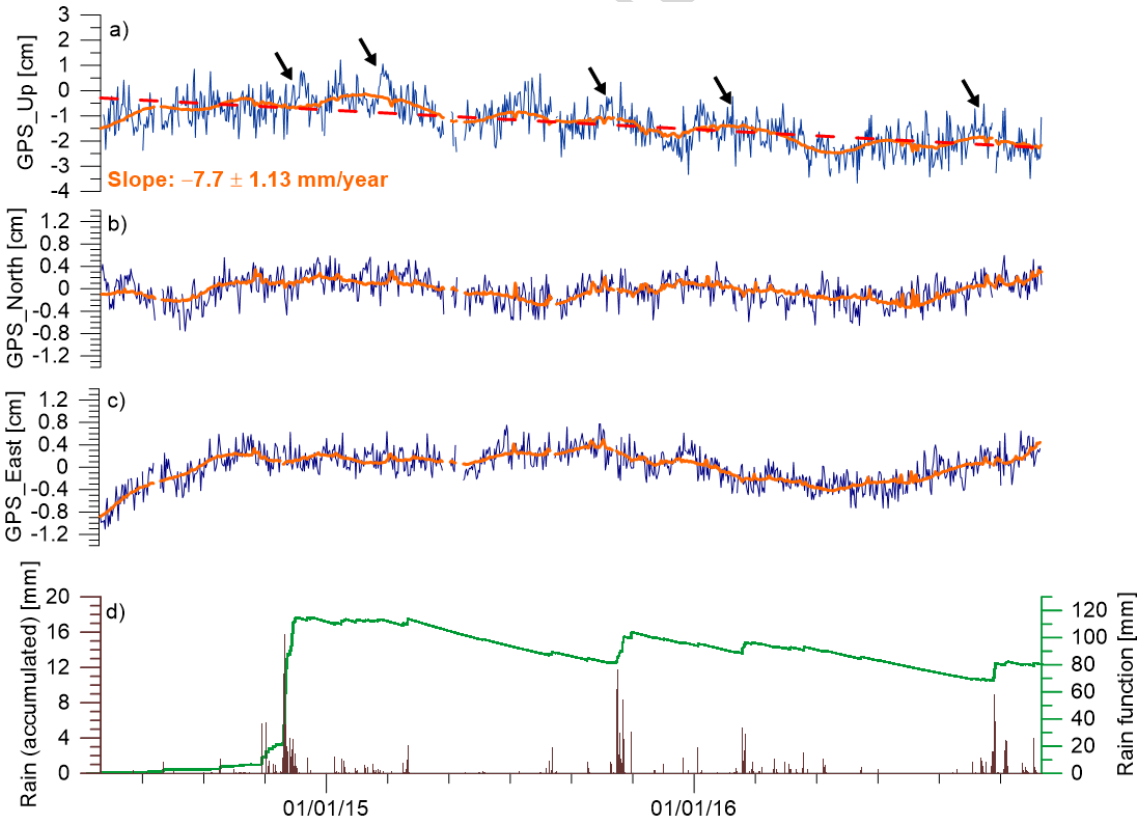

Fig. 8: Up, North and East displacements (a, b, c, respectively) computed for CAME station. Modelling curve (continuous thick orange line) of the respective displacement, S(t), according to the approach of equation (2). Linear fit (dashed red line) of the modelled curve S(t) for the vertical displacement (vertical rate displacement "Slope" is given too). Accumulated rain (d) at the laboratory of Camelleros (GLL), and the results of convolving the rainfall data with the exponential function of equation (5); the arrows in panel A highlight the transient vertical displacement due to rainfall.

3. DISCUSSION

The time evolution of room temperature at LC-GLL (Fig. 6b), likely related to the heat transfer from the surrounding geothermal anomalies at depth, displays a regular increase starting in 2003 and lasting about 7 years, then it stabilizes since 2010. This period can be divided in three different ones (indicated as P1, P2, and P3 in Fig. 6), before, during and after the abnormal temperature raise experienced at LC-GLL. Looking more closely at the correlation between strain/tilt signals and the modelled thermal function (Eq. 2), we are able to retrieve some regularities in the observed trends. For tilt measurements, the regression coefficients (Tab. 4) clearly change during P2 when temperature increases significantly, amounting to about 20 °C. After the temperature stabilization, during P3, the obtained regression values are similar to the ones for P1. For the strain measurements, the regression coefficients obtained stand for ground deformation produced by temperature changes at LC-GLL. Thus, the regression coefficient for the direction TD shows a significant variation from P1 to P2, and for period P3 is about 2.2 times larger than the value obtained for P1. For strains in LD direction, the regression coefficient also varies from P1 to P2, coinciding with the temperature increase at GLL, and the value obtained for P3 is about 3.4 times larger than for P1. All these values confirm that the deformation pattern is sensitive to the thermoelastic strains produced by the large increase of temperature observed between 2003 and 2010 at LC-GLL.

We can get additional insights from the analysis of correlation between the observed ground deformation and the rain function (Eq. 5). The correlation for ground tilt at LC-GLL provides similar coefficients for both LD and TD directions, amounting to about 0.9, 0.7 and 0.3 for the years 2014, 2015 and 2016, respectively. Likewise, the correlation coefficients turning out for strain measurements are similar for both LD and TD directions, for years 2014 (0.8) and 2015 (0.7), whereas in the year 2016 is lower for TD (0.5) and it is not significant at LD (<0.3). Similarly, the correlation coefficient for the vertical component of GNSS displacement at CAME site ranges between 0.3 (year 2015) and 0.2 (years 2014 and 2016). However, correlation coefficients for horizontal components of GNSS displacement (North and East) are higher than the vertical one and range between 0.5 and 0.8 during all the observing period.

The modeled curves, S(t), for tilts and strains following the regression approach given by equation (2), demonstrate that rainfall also induces changes in tilts and strains recorded at LC-GLL for the same period of GNSS observations at CAME site (Fig. 9). Similarly, precipitation effects and hydrological induced signals on ground based observations were observed and modelled at the Geodynamic Observatory of Moxa in Germany (Kroner and Jahr, 2006; Jahr et al., 2009).

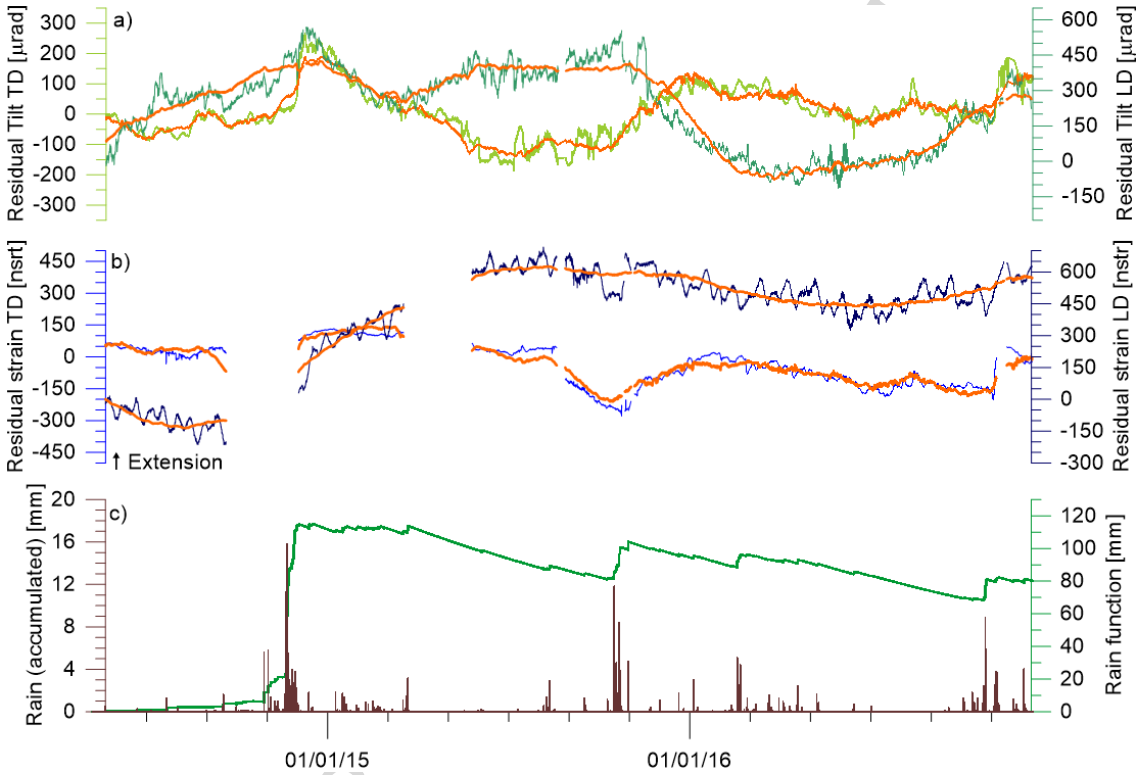

Fig. 9: Residual tilt and extension (a, b) computed for directions TD and LD, after removing tides and room temperature effects at tidal frequencies in the laboratory of Camelleros (GLL). The thick orange lines represent the modelling curves of the respective tilts and extensions, S(t), according to the approach of equation (2). Panel (c) shows the precipitation accumulated at GLL, and the results of convolving the rainfall data with the exponential function of equation (5).

Absolute velocities in ITRF08 for each station of Lanzarote network can be retrieved from the linear trends envisaged in the daily GNSS time series of the horizontal (North/East) components (Fig. 2). All the stations, except CAME and YAIZ, show negligible vertical trends. CAME displays a significant subsidence at a rate of 6.4 ± 0.8 mm/year and YAIZ experiences a subsidence too, but at smaller rate (2.6 ± 0.6 mm/year). These outcomes are quite in agreement with InSAR data [see Fig. 9 in González and Fernández 2011] discussed by Fernández et al. (2015). These authors report a linear velocity deformation map in the TVA area with maximum subsidence

rates up to 6 mm/year, as we find in CAME. Indeed, González and Fernández (2011) also reported line-of-sight movement away from the satellite of ~2.5 mm/year, which is consistent with the subsidence detected at YAIZ GNSS site. However, the uncertainties in the InSAR results is likely higher in that region (González and Fernández, 2011). However, it's noteworthy that InSAR data span the period (1992 to 2000), while our GNSS ones span 2014-2017, hence some steady-state process, active for at least 25 years, can be envisaged implying such a regular trend.

Furthermore GNSS time series clearly display a relevant variability just at CAME station occurring some months after the installation, namely during October-November 2014 (Figs. 2, 3 and 4). This seems to be correlated to an anomalous heavy raining period, which could have very locally affected the heat transfer from the thermal sources due to a more intense water circulation in the close neighboring of the main geothermal anomaly.

The velocity solutions (Fig. 5) we retrieve are referred to different frames: absolute velocities in ITRF08 and "local" frame, the latter obtained by computing relative velocities with respect to TIAS station. In order to find out local tectonics in TVA area, we compute local velocity with respect to TIAS, which is the closest to TVA and shows a negligible vertical trend as well as a horizontal velocity coherent with ITRF08. As expected, the velocities are coherent to the known ones for the different frames except for CAME showing a residual velocity amounting to about 3 mm/year pointing towards SE. This result is also confirmed by the baseline CAME-TIAS showing a shortening (Fig. 4). The velocities in each frame are summarized in Table 3. As previously mentioned, there exist areas with thermal anomalies located at TVA (Fig. 1) whose origin likely rely on a batch of relic hot magma of 1730-1736 eruption located at a depth (Araña et al., 1984). The heat transfer is mainly produced by hydrothermal fluids raising through existing fractures in the Earth's crust (Araña et al, 1984; Carracedo and Troll, 2016). Alterations in the heat sources can generate variations in the surface anomalies. That is the case experienced in the LC-GLL at TVA, where room temperature recorded was increasing by about 20 ºC during 7 years, since 2003 (Fig. 6). Consequently, a ground deformation pattern, as measured with extensometers and tiltmeters installed therein, was interpreted as related to the surface manifestations of thermal anomalies in this area (Arnoso et al., 2012b).

4. CONCLUSIONS

We have produced an improved monitoring of ground deformation of Timanfaya volcanic area (TVA), an interesting sector of Lanzarote Island, where the highest geothermal anomalies take place. Our study rely on the use of three continuous geodetic techniques, in fact, we analyze some 3 years of continuous GNSS data collected on a small network deployed on the island as well as nearly 20 years of tiltmeter and strainmeter records acquired at Los Camelleros Laboratory (LC-GLL). We take a closer look at the origin of the observed deformations through a correlation analysis between the geodetic records and two response functions built up from temperature and rain data collected in the laboratory.

The main results can be summed up as follows:

The GNSS time series clearly display a relevant variability just at CAME site occurring during the fall 2014, some months after the installation. Our correlation analysis applied to this event unveils a time overlap with an anomalous heavy raining period, which could have played a role affecting the efficiency of the heat transfer from the underground. Moreover, we retrieve GNSS velocity solutions mapped in two different frames: absolute velocities in ITRF08 and "local" frame, which defines velocities relative to one point (TIAS) being close to TVA, but outside the main geothermal area. By the way of the latter framing we are able to highlight the local active tectonics in the surroundings of CAME site. The retrieved velocities appear to be coherent to the known ones for the different frames except for CAME showing a residual velocity amounting to about 3 mm/year pointing towards SE. This result even matches the time evolution of the baseline CAME-TIAS showing a shortening (Fig. 4). All the stations, except CAME and YAIZ, present negligible vertical trends. CAME site is going to experience a significant subsidence at a rate of 6.4 ± 0.8 mm/year. The same occurs for YAIZ, but at smaller rate (2.6 ± 0.6 mm/year). As matter of fact, these outcomes quietly agree with some previous InSAR data (González and Fernández, 2011) discussed by Fernández et al. (2015), who reconstructed a linear velocity deformation map in the TVA with a subsidence rates up to 6 mm/year as well as some 2.5 mm/year subsidence for a second pixel not far from YAIZ site.

The geodetic observations lead us to try to draw a coherent framework where hydrothermal fluids and infiltration water play a key role in the very localized ground deformation detected in that sector of TVA. Indeed to get a quantitative modelling a detailed monitoring of the aquifers and water tables would be needed.

We think that the recorded tilt/strain signals at LC-GLL since 2003 and later the ground displacements measured with GNSS, could be linked with variations in surface thermal anomalies, most probably related with movement of hydrothermal fluids. Actually, there are evidences that thermal anomalies at TVA are varying due to fluctuations in the water table, which is altered by rainy periods. Heavy rain can improve the infiltration rate of the meteoric water increasing the efficiency of thermal transfer from the underground heat source. Seasonal rains or episodic heavy rains, as in fall 2014, can vary the water table, which is in contact with or near to the intruded magma bodies, and, as a feedback effect, trigger the transport of energy through the fractures by water vapour. Even the significant subsidence observed at CAME and the slighter one at YAIZ could be related with the interaction between the aquifers and the volcanic system around TVA, still in a cooling (and/or crystallization) phase after the 1730-1736 eruption and responsible for the very high surficial geothermal gradient.

ACKNOWLEDGEMENTS

Projects CGL2015-63799-P of Spanish Ministry of Economy and Competitiveness, and 320/2011 of National Parks Autonomous Agency have supported this research. The authors are greatly indebted to Jaime Arranz and Orlando Hernández, from Casa de los Volcanes-Cabildo Insular of Lanzarote. Special thanks to the staff of National Park of Timanfaya. Last but not least we acknowledge Thomas Jahr and an anonymous reviewer who thoroughly commented on the paper.

REFERENCES

Altamimi Z., Collilieux X., Métivier L. (2011). ITRF2008: An improved solution of the international terrestrial reference frame. Journal of Geodesy, 85 (8), 457-473, doi:10.1007/s00190-011-0444-4.

Amoruso A., Crescentini L., Scarpa R., Bilham R., Linde A. T., Sacks I. S. (2015). Abrupt magma chamber contraction and microseismicity at Campi Flegrei, Italy: Cause and effect determined from strainmeters and tiltmeters. J Geophys. Res. Solid Earth, 120, 5467–5478, doi:10.1002/2015JB012085.

Anguita F., Hernán F. (1975). A propagating fracture model versus a hot spot origin for the Canary Islands. Earth Planet. Sci. Lett., 27, 11-19.

Anguita F.J., Hernán F. (2000). The Canary Islands origin: a unifying model. Journal of Volcanology and Geothermal Research, 103, 1-26.

Araña V., Ortiz R. (1984). Volcanología. CSIC, Madrid, 510 pp.

Araña V., Diez-Gil J., Ortiz R., Yuguero J. (1984). Convection of Geothermal Fluids in the Timanfaya Volcanic Area (Lanzarote, Canary Islands). Bulletin of Volcanology, 47, 667-677.

Araña V., Ortiz R. (1991). The Canary Islands: tectonics, magmatism and geodynamic framework. In: Kampunzu, A., Lubala, P. (Eds.), Magmatism in Extensional Structural settings. The Phanerozoic African Plate, Springer, Berlin, pp. 209-249

Arnoso J., Fernández J., Vieira R. (2001a). Interpretation of tidal gravity anomalies in Lanzarote, Canary Islands. Journal of Geodynamics, 31, 341–354.

Arnoso J., Vieira R., Vélez E., Cai W., Tan S., Jiang J., Venedikov A. P. (2001b). Monitoring tidal and non-tidal variations in Lanzarote Island (Spain). Journal of the Geodetic Society of Japan, 47 (1), 456–462.

Arnoso J., Benavent M., Montesinos F. G. (2011). Updating gravimetric tide parameters and ocean tide loading corrections at the observing sites Cueva de los Verdes and Timanfaya of LGL. In R. Vieira Díaz and E. J. Vélez Herranz (Eds.). 25 años de actividad científica en el Laboratorio de Geodinámica de Lanzarote: Casa de los Volcanes - Cabildo de Lanzarote.

Arnoso J., Montesinos F. G., Benavent M., Vélez E. J. (2012a). The 2011 volcanic crisis at El Hierro (Canary Islands): monitoring ground deformation through tiltmeter and gravimetric observations, Geophysical Research Abstracts, 14, EGU2012–5373.

Arnoso J., Vélez E., Soler V., Montesinos F. G., Benavent M. (2012b). The Lanzarote Geodynamic Laboratory: new capabilities for monitoring of volcanic activity at Canary Islands. Geophysical Research Abstracts, Vol. 14, EGU2012-10054.

Battaglia M., Segall P., Murray J., Cervelli P., Langbein J. (2003a). The mechanics of unrest at Long Valley caldera, California: 1. Modeling the geometry of the source using GPS, leveling and two-color EDM data. Journal of Volcanology and Geothermal Research, 127, 195-217, doi:10.1016/S0377-0273(03)00170-7.

Battaglia M., Segall P., Roberts C. (2003b). The mechanics of unrest at Long Valley caldera, California. 2. Constraining the nature of the source using geodetic and micro-gravity data. Journal of Volcanology and Geothermal Research, 127, 219-245, doi:10.1016/S0377-0273(03)00171-9.

Boehm J., Werl B., Schuh H. (2006). Troposphere mapping functions for GPS and very long baseline interferometry from European Centre for Medium-Range Weather Forecasts operational analysis data. J. Geophys. Res., 111, B02406, doi:10.1029/2005JB003629.

Bonaccorso A., Aloisi M. and Mattia M. (2002). Dike emplacement forerunning the Etna July 2001 eruption modeled through continuous tilt and GPS data. Geophys. Res. Lett., 29, 13, 1624, doi:10.1029/2001GL014397.

Bonaccorso A., Bonforte A., Gambino S., Mattia M., Guglielmino F., Puglisi G., Boschi E. (2009). Insight on recent Stromboli eruption inferred from terrestrial and satellite ground deformation measurements. Journal of Volcanology and Geothermal Research, 182, 172–181, doi:10.1016/j.jvolgeores.2009.01.007.

Bonaccorso A., Currenti G., Linde A., Sacks S. (2013). New data from borehole strainmeters to infer lava fountain sources (Etna 2011–2012). Geophys. Res. Lett., 40, 3579–3584, doi:10.1002/grl.50692.

Carracedo J. C., Rodríguez Badiola E. R., Soler V. (1992). The 1730-1736 eruption of Lanzarote: an unusually long, high magnitude fissural basaltic eruption in the recent volcanism of the Canary Islands. Journal of Volcanology Geothermal Research, 53, 239-250.

Carracedo J. C. and Troll V. (2016). The geology of Canary Islands. 621 pp. Elsevier, Amsterdam.

Chang W. L., Smith R. B., Farrell J., Puskas C. M. (2010). An extraordinary episode of Yellowstone caldera uplift, 2004–2010, from GPS and InSAR observations, Geophys. Res. Lett., 37, L23302, doi:10.1029/2010GL045451.

Crescentini L., Amoruso A. (2007). Effects of crustal layering on the inversion of deformation and gravity data in volcanic areas: An application to the Campi Flegrei caldera, Italy, Geophys. Res. Lett., 34, L09303, doi:10.1029/2007GL029919.

Crossley D., Xu H., Van Dam T. (1998). Comprehensive analysis of 2 years of SG data from Table Mountain, Colorado. In: Ducarme B., Pâquet P. (Eds.) Proc. 13th Symposium on Earth Tides, Brussels 1997, 659–68.

Dañobeitia J. J., Canales, J. P. (2000). Magmatic underplating in the Canary Archipelago. Journal of Volcanology and Geothermal Research, 103, 27–41.

DeMets C., Gordon R. G., Argus D. F., Stein S. (1994). Effect of recent revisions to the geomagnetic reversal time scale on estimates of current plate motions, Geophys. Res. Lett., 21, 2191-2194, doi:10.1029/94GL02118.

Díez-Gil J. L., Araña V., Ortíz R., Yuguero J. (1987). Stationary convection model for heat transport by means of geothermal fluids in post eruptive systems. Geothermics, 15, 77-87.

Dong D. N., Herring T. A., King R. W. (1998). Estimating regional deformation from a combination of space and terrestrial geodetic data. Journal of Geodesy, 72, 200–214.

Dzurisin D. (2003). A comprehensive approach to monitoring volcano deformation as a window on the eruption cycle. Reviews of Geophysics 41, doi: http://dx.doi.org/10.1029/2001RG000107.

Dzurisin D. (2007). Volcano Deformation. Geodetic Monitoring Techniques. 441 pp., Springer.

Fernández J., Vieira R., Díez J., Toro C. (1992). Investigations on crustal thickness, heat flow and gravity tide relationship in Lanzarote island. Physics of the Earth and Planetary Interiors, 74 (3‑4), 199‑208, doi:10.1016/0031-9201(92)90010-S.

Fernández J., Gonzalez P. J., Camacho A. G., Prieto J. F., Brù G. (2015). An Overview of Geodetic Volcano Research in the Canary Islands. Pure and Applied Geophysics, 172, 3189-3228, doi: 10.1007/s00024-014-0916-6.

Fúster J. M. (1975). Las Islas Canarias: un ejemplo de evolución espacial y temporal del vulcanismo oceánico. Estudios Geológicos 31, 439–463.

Gambino S., Aloisi M., Falzone G., Ferro A. (2016). Tilt signals at Mount Melbourne, Antarctica: evidence of a shallow volcanic source Polar Research 2016, 35, 28269, dx.doi.org/10.3402/polar.v35.28269.

González P. J., J. Fernández (2011), Error estimation in multitemporal InSAR deformation time series, with application to Lanzarote, Canary Islands, J. Geophys. Res., 116, B10404, doi:10.1029/2011JB008412.

Grapenthin R., Freymueller J. T., Kaufman A. M. (2013). Geodetic observations during the 2009 eruption of Redoubt Volcano, Alaska. Journal of Volcanology and Geothermal Research, 259, 115–132, doi: 10.1016/j.jvolgeores.2012.04.021.

Guillou H., Carracedo J. C., Perez Torrado F., Rodríguez Badiola E. (1996). K–Ar ages and magnetic stratigraphy of a hotspot induced, fast grown oceanic island: El Hierro, Canary Islands. Journal of Volcanology Geothermal Research, 73, 141–155.

Herring T. A. (2003). MATLAB Tools for viewing GPS velocities and time series. GPS Solutions, 7 (3), 194–199.

Herring T. A., King R. W., Floyd M. A., McClusky R. W. (2015a). Gamit-Reference Manual. Release 10.6; pp. 168.

Herring T. A., King R. W., Floyd M. A., McClusky R. W. (2015b). Globk-Reference Manual. Release 10.6; pp. 95.

Hoernle K., Carracedo J. C. (2009). Canary Islands, Geology. In: Gillespie R, Clague DA (eds) Encyclopedia of islands. University of California Press, Berkeley, pp 133-143.

Jahr T., Jentzsch G., Weise A., (2009). Natural and man-made induced hydrological signals, detected by high resolution tilt observations at the Geodynamic Observatory Moxa/Germany. Journal of Geodynamics 48, 126–131.

Kümpel H. J., Lehmann K., Fabian M., Mentes G. (2001). Point stability at shallow depth — experience from tilt measurements in the lower Rhine embayment, Germany, and implications for high resolution GPS and gravity recordings. Geophysical Journal International, 146, 699–713.

Kroner C., Jahr T. (2006). Hydrological experiments around the superconducting gravimeter at Moxa Observatory, Journal of Geodynamics, 41(1–3), 268–275, doi:10.1016/j.jog.2005.08.012.

Lagler K., Schindelegger M., Böhm J., Krásná H., Nilsson T. (2013). GPT2: Empirical slant delay model for radio space geodetic techniques. Geophys. Res. Lett., 40 (6), 1069-1073, doi:10.1002/grl.50288.

Langbein J. O., Burford R. O., Slater L. E. (1990). Variations in fault slip and strain accumulation at Parkfield, California: Initial results using two-color Geodimeter measurements. 1984-1988. J. Geophys. Res., 95, 2533-2552.

Le Mével H., Feigl K. L., Cordova L., DeMets C., Lundgren P. (2015). Evolution of unrest at Laguna del Maule volcanic field (Chile) from InSAR and GPS measurements, 2003 to 2014. Geophys. Res. Lett., 42, 6590–6598, doi:10.1002/2015GL064665.

López C., Blanco M. J., Abella R., Brenes B., Cabrera Rodríguez V. M. et al. (2012) Monitoring the volcanic unrest of El Hierro (Canary Islands) before the onset of the 2011–2012 submarine eruption. Geophys. Res. Lett., 39, L13303. doi:10.1029/2012GL051846.

López C., Benito-Saz M. A., Martí J., del-Fresno C., García-Cañada L., Albert H., Lamolda H. (2017). Driving magma to the surface: The 2011–2012 El Hierro Volcanic Eruption, Geochem. Geophys. Geosyst., 18, doi:10.1002/2017GC007023.

Lyard F., Lefevre F., Letellier T., Francis O. (2006). Modelling the global ocean tides: modern insights from FES2004. Ocean Dynamics, 56, 394-415. doi: 10.1007/s10236-006-0086-x.

McDougall I., Schmincke H. U. (1976). Geochronology of Gran Canaria, Canary Islands: Age of shield building volcanism and other magmatic phases. Bulletin of Volcanology, 40, 1-21.

Mezcua J., Buforn E., Udías A., Rueda J. (1992). Seismotectonics of the Canary Islands. Tectonophysics, 208, 447-452.

Montgomery-Brown E. K., Sinnett D. K., Larson K. M., Poland M. P., Segall P., Miklius A. (2011). Spatiotemporal evolution of dike opening and décollement slip at Kilauea Volcano, Hawai'i. J. Geophys. Res., 116, B03401, doi:10.1029/2010JB007762.

Morgan W. J. (1971) Convection plume in the lower mantle. Nature 230:42–44.

Newman A. V., Stiros S., Feng L., Psimoulis P., Moschas F., Saltogianni V., Jiang Y., Papazachos C., Panagiotopoulos D., Karagianni E., Vamvakaris D. (2012). Recent geodetic unrest at Santorini Caldera, Greece, Geophys. Res. Lett., 39, L06309, doi:10.1029/2012GL051286.

Nikolaidis (2002). Observation of geodetic and seismic deformation with the Global Positioning System. Ph.D. thesis, University of California, San Diego

Owen S., Segall P., Lisowski M., Miklius A., Denlinger R., Sako M. (2000). Rapid deformation of Kilauea Volcano: Global positioning system measurements between 1990 and 1996. J. Geophys. Res., 105, B8, 18983–18998, doi:10.1029/2000JB900109.

Puglisi G., Bonforte A., Maugeri S. R. (2001). Ground deformation patterns on Mt. Etna, between 1992 and 1994, inferred from GPS data. Bulletin of Volcanology, 62:371–384.

Sainz-Maza S., Arnoso J., Gonzalez F. G., Martí J., (2014). Volcanic signatures in time gravity variations during the volcanic unrest on El Hierro (Canary Islands). J. Geophys. Res. Solid Earth, 119, 5033–5051, doi:10.1002/2013JB010795.

Sturkell M., Einarsson P., Sigmundsson F., Geirsson H., Ólafsson H., Pedersen R., de Zeeuw-van Dalfsen E., Linde T. A., Sacks S. I., Stefánsson R. (2006). Volcano geodesy and magma dynamics in Iceland. Jornal of Volcanoly and Geothermal Research, 150, 14-34, doi:10.1016/j.jvolgeores.2005.07.010.

Tammaro U., De Martino P., Obrizzo F., Brandi G., D'Alessandro A., Dolce M., Malaspina S., Serio C., Pingue F. (2013). Somma Vesuvius volcano: ground deformations from CGPS observations (2001-2012). Annals of Geophysics, 56, 4, 2013, S0456; doi:10.4401/ag-6462.

Vélez E. J., Vieira R., Arnoso J., Cai W., Jiang J., Tan S. (2001). Tidal and non-tidal observations in a volcanic active region. Journal of the Geodetic Society of Japan, 47 - 1, pp. 488 - 493.

Venedikov A. P., Arnoso J., Cai W., Vieira R., Tan S., Vélez E. J. (2006). Separation of the long-term thermal effects from the strain measurements in the Geodynamics Laboratory of Lanzarote. Journal of Geodynamics, 41 (1-3), 213-220.

Vieira R., van Ruymbecke M., Fernández J., Toro C. (1991). The Lanzarote Underground Laboratory. Cahiers du Centre Européen de Géodynamique et de Séismologie, 4, 71‑86.

Vieira R., Vélez E. J. (2006). Guía del Laboratorio de Geodinámica de Lanzarote. Publicaciones del Instituto de Astronomía y Geodesia (CSIC-UCM). 201, pp. 1 – 60

Widiwijayanti, C., Clarke, A., Elsworth D. and Voight, B. (2005). Geodetic constraints on the shallow magma system at Soufrière Hills Volcano, Montserrat. Geophys. Res. Lett.,, Vol. 32, L11309, doi: 10.1029/2005GL022846.

Williams S. D. P., Bock Y., Fang P. (1998). Integrated satellite interferometry: Tropospheric noise, GPS estimates and implications for interferometric synthetic aperture radar products, J. Geophys. Res., 103, 27,051–27,067.

Williams S. D. P., Bock Y., Fang P., Jamason P., Nikolaidis R. M., Prawirodirdjo L., Miller M., Johnson D. J. (2004). Error analysis of continuous GPS position time series. J. Geophys. Res., 109, B03412, doi: 10.1029/2003JB002741.

Wilson J. T. (1963). Continental drift. Scientific American, 208, 86–100.

Zadro M., Braitenberg C. (1999). Measurements and interpretation of tilt-strain gauges in seismically active areas. Earth Science Reviews. 47, 151–187.

HIGHLIGHTS

- Timanfaya Volcanic Area (Lanzarote –Canary Islands) hosts the most intense geothermal anomaly of the island.
- A detailed geodetic study is carried out by means of three years of GNSS data collected on a small network and nearly 20 years of tiltmeter and strainmeter records.
- The deformation patterns and the environmental observations (rainfall and temperature) leads to a qualitative model of the interplaying role between the hydrological systems and the geothermal anomalies.
- The deformation scenario is due to the enhancement of the thermal transfer from the underground heat source driven by the infiltration of meteoric water.